JOURNAL OF GEOPHYSICAL RESEARCH, VOL. 112, B11101, doi:10.1029/2007JB004963, 2007

Eocene-Oligocene paleoceanographic changes in the stratotype section, Massignano, Italy: Clues from rock magnetism and stable isotopes

Luigi Jovane,[1] Mario Sprovieri,[2] Fabio Florindo,[1] Gary Acton,[3] Rodolfo Coccioni,[4] Barbara Dall'Antonia,[5] and Jaume Dinarès-Turell[1]

Received 30 January 2007; revised 15 July 2007; accepted 16 August 2007; published 10 November 2007.

[1] We have conducted high-resolution paleomagnetic and rock magnetic studies, in addition to stable isotope analyses of the Massignano sedimentary section, which is the Global Stratotype Section and Point (GSSP) for the Eocene-Oligocene boundary. Our research builds upon the many past studies of the Massignano section in seeking to understand the timing and nature of the paleoenvironmental variations that occurred during the transition for the Earth's climate system from greenhouse to icehouse. The new paleomagnetic results provide a refined magnetostratigraphy of the section and new age for the Eocene-Oligocene boundary at 33.7 Ma. Abrupt and large alternations in magnetic, concentration, composition, and grain sizes that occur in the high-resolution rock magnetic record are interpreted to be the result of rapid bimodal shifts in deep-sea circulation that affect sediment sources or transport. We speculate that currents flowing through the gateway between the Atlantic and Indo-Pacific Oceans may have turned on and off as the gateway was progressively closing, resulting in the deposition of two different assemblages of magnetic minerals at Massignano. Finally, stable isotope ($\delta^{18}O$ and $\delta^{13}C$) data collected on ostracod valves also suggest significant changes in sea bottom circulation in the Neo-Tethys Ocean at and about 2 m.y. before the Eocene-Oligocene boundary.

Citation: Jovane, L., M. Sprovieri, F. Florindo, G. Acton, R. Coccioni, B. Dall'Antonia, and J. Dinarès-Turell (2007), Eocene-Oligocene paleoceanographic changes in the stratotype section, Massignano, Italy: Clues from rock magnetism and stable isotopes, *J. Geophys. Res.*, *112*, B11101, doi:10.1029/2007JB004963.

1. Introduction

[2] A transition in the Earth's climatic system occurred from the middle-late Eocene to early Oligocene, when the greenhouse climate that characterized most of the Cretaceous evolved to icehouse conditions [e.g., *Zachos et al.*, 1994, 2001; *Lear et al.*, 2000; *Miller et al.*, 2005a, 2005b]. In close proximity to the Eocene-Oligocene (E/O) boundary, the "Oi-1" cooling event [*Miller et al.*, 1991] at ~33.55 Ma marks a significant deterioration of the global climate in the Cenozoic. This event is part of a long-term increase in $\delta^{18}O$ reflecting a combination of global cooling and ice growth in Antarctica [e.g., *Zachos et al.*, 1996; *Kennett and Shackleton*, 1976]. The Oi-1 event has been attributed to changes in atmospheric CO_2 concentration during the greenhouse-icehouse transition [*DeConto and Pollard*, 2003; *Pagani et al.*, 2005] or, alternatively, to the opening of the Southern Ocean Gateways [*Barker and Thomas*, 2004; *Barker et al.*, 2007; *Livermore et al.*, 2005, 2007; *Lawver and Gahagan*, 2003].

[3] The climate proxy records throughout the Eocene indicate warm and stable tropical sea surface temperatures [*Pearson et al.*, 2001; *Tripati et al.*, 2003, 2005] with the exception of short and abrupt cooling steps at 48, 45, and 42 Ma recorded from planktonic foraminiferal Mg/Ca data [*Tripati et al.*, 2003]. Nannofossil and foraminifera assemblages, dinoflagellate cyst, palynology, clay mineralogy, and oxygen isotopes indicate that the foremost cooling event at the Eocene-Oligocene boundary was preceded by separate cooling pulses in the Eocene [e.g., *Diester-Haass and Zahn*, 1996; *Vonhof et al.*, 2000; *Bohaty and Zachos*, 2003; *Jovane et al.*, 2004], prorated by relatively stable warming periods. These cooling pulses may have marked the initial stages toward modern thermohaline circulation.

[4] The Massignano section represents the Global Stratotype Section and Point (GSSP) for the Eocene-Oligocene boundary [*Premoli Silva and Jenkins*, 1993; and discussions of *Brinkhuis and Visscher*, 1995], where many multidisciplinary studies have been carried out [see *Jovane et al.*, 2004, 2006 and references therein]. Previous magnetostrati-

[1]Istituto Nazionale di Geofisica e Vulcanologia, Rome, Italy.
[2]Istituto Ambiente Marino Costiero (CNR), Calata Porta di Massa (Interno Porto di Napoli), Naples, Italy.
[3]Department of Geology, University of California, Davis, Davis, California, USA.
[4]Istituto di Geologia e Centro di Geobiologia, Università degli Studi di Urbino "Carlo Bo", Campus Scientifico Località Crocicchia, Urbino, Italy.
[5]Università di Pisa, Dipartimento di Scienze della Terra, Pisa, Italy.

0148-0227/07/2007JB004963$09.00

graphic interpretations [*Bice and Montanari*, 1988; *Lowrie and Lanci*, 1994; *Lanci et al.*, 1996; *Lanci and Lowrie*, 1997; *Lanci et al.*, 1998] contain intervals that were poorly resolved and some conflicting interpretation. Similarly, isotope data collected throughout the section by *Bodiselitsch et al.* [2004] were determined on bulk samples that may reflect signals from many different sources, making them more difficult to interpret directly in terms of paleoceanographic and paleoclimate conditions.

[5] In this paper, we present new high-resolution magnetostratigraphic data and a stable isotope record (collected from moderately well-preserved ostracod valves) in order to: (1) enlarge the age model for the stratotype section, (2) recognize the most relevant sedimentary and environmental variations that occurred in the late Eocene and the early Oligocene at Massignano, and (3) interpret the variations in terms of changes in paleoceanographic and paleoclimate conditions.

2. Geological Setting and Stratigraphy

[6] The Massignano section (http://www.stratigraphy.org/eocoli.htm) is located in the Monte Conero area on the Adriatic coast of central Italy. The GSSP section (43°32′13″N; 13°35′36″E) is exposed in an abandoned quarry on the 'Strada Provinciale del Conero' near the village of Massignano, a few kilometers south of Ancona. The Massignano sedimentary succession belongs to the Umbria-Marche sedimentary basin, which was deposited in a lower bathyal depositional setting of the Neo-Tethys realm at a paleodepth of 1000–1500 m [*Coccioni and Galeotti*, 2003].

[7] The Monte Conero promontory lies in the outer and younger part of the Umbria-Marche Apennines, that is an arcuate fold-and-thrust belt developed during the Neogene, following the closure of the Mesozoic Tethys Ocean and the deformation of the Adria (i.e., African) passive continental margin.

[8] The Massignano Section is 23 m-thick and composed of the Scaglia Variegata Formation in the lower part and of the Scaglia Cinerea Formation in the upper part. The Scaglia Variegata Formation consists of alternating reddish/greenish-gray marls and calcareous marls from the top of the early Eocene to the end of the late Eocene. In the Umbria-Marche Basin, the Scaglia Variegata Formation is composed of three members: the lower consists of 50 m of red-violet limestone layers that are 15–100 cm thick and violet marl layers that are 20–200 cm thick with intercalations of white marl layers; the middle member contains 20 m of marly limestones and yellow-green and gray marls that are 15–35 cm thick; the upper member consists of 7 m of red calcareous marl layers, each about 15 cm thick. The Scaglia Variegata Formation grades upward into gray marls and marly limestones of the Scaglia Cinerea Formation, which was mostly deposited during the Oligocene. The boundary between the upper member of the Scaglia Variegata Formation and the Scaglia Cinerea Formation occurs at 12 msl (meters stratigraphic level from the base) [*Coccioni et al.*, 1988]. Note that all the positions in the section are measured from the base in msl.

[9] The geological record spans the interval from the latest Eocene to the early Oligocene [e.g., *Lowrie and Lanci*, 1994; *Lanci and Lowrie*, 1997]. The Eocene-Oligocene boundary occurs in the lower part of the Scaglia Cinerea Formation, at a stratigraphic level of 19 msl [*Premoli Silva et al.*, 1988; *Premoli Silva and Jenkins*, 1993]. Several biotite-rich levels of volcanic origin (e.g., 5.90, 6.20, 7.30, 7.70, 12.00 msl) occur through the section and three iridium-rich layers occur at 5.65, 6.17 and 10.28 msl, which are related to impactoclastic events [*Montanari et al.*, 1988, 1993; *Montanari and Koeberl*, 2000; *Bodiselitsch et al.*, 2004]. Biostratigraphically, the Massignano section spans the planktonic foraminiferal Zone P15 to P18 [*Coccioni et al.*, 1988, 2000; *Spezzaferri et al.*, 2002] and calcareous nannoplankton Zones from NP18 to NP21 [*Coccioni et al.*, 1988, 2000; *Monechi et al.*, 2000].

3. Previous Studies

3.1. Magnetostratigraphy

[10] *Lowrie and Lanci* [1994] conducted a paleomagnetic investigation on the Massignano section refining the previous magnetostratigraphy [*Bice and Montanari*, 1988] (Figure 1). They collected 32 unevenly spaced samples over the entire section. The samples were subjected to progressive thermal and alternated field (AF) demagnetization in order to identify the characteristic remanent magnetizations (ChRM) components. AF demagnetization revealed multiple components, often with overlapping coercivity spectra, and the presence of an unresolved high-coercivity component. The ChRM component was generally well defined from different components [*Lowrie and Lanci*, 1994] using thermal demagnetization for 29 samples (Figure 1). The presence of mixtures of magnetic minerals was observed from progressive acquisition of isothermal remanent magnetization (IRM) and thermal demagnetization of a composite IRM [*Lowrie*, 1990]. The results indicated that magnetite was the main magnetic carrier over the section and that hematite occurred as a secondary magnetic mineral in the upper Scaglia Variegata Formation. The same authors in a different study [*Lanci et al.*, 1996] compared the Massignano section with the MASSICORE (42° 32′ 09.6″N; 13° 35′ 34.3″E), which is a 39.4 m-long and 10 cm diameter core, drilled just 110 m south from the Massignano quarry. The MASSICORE magnetic polarity zonation [*Lanci et al.*, 1996; *Lanci and Lowrie*, 1997; *Lanci et al.*, 1998] obtained from 253 of the 260 samples collected span from C12r to C16n.2n (Figure 1).

[11] Based on the "African" apparent polar wander reference path of *Besse and Courtillot* [1991] the Early Oligocene expected direction at Massignano has a declination of 6° (the observed declination was 13°) and an inclination of 56°. At Massignano, *Lowrie and Lanci* [1994] noted a clockwise rotation of 7° and an inclination that was 11° shallower than expected (the observed inclination was 45°). *Lanci et al.* [1996] determined a mean declination of 9.5° and a mean inclination of 39° (α_{95} = 2.5; κ = 12.67) for MASSICORE, with the normal polarity samples giving a declination of 4° and inclination of 40° and the reversed polarity samples giving a declination of 192° and an inclination of −38°.

3.2. Stable Isotopes

[12] The occurrence of impactoclastic layers throughout the Massignano sedimentary record attracted the consideration

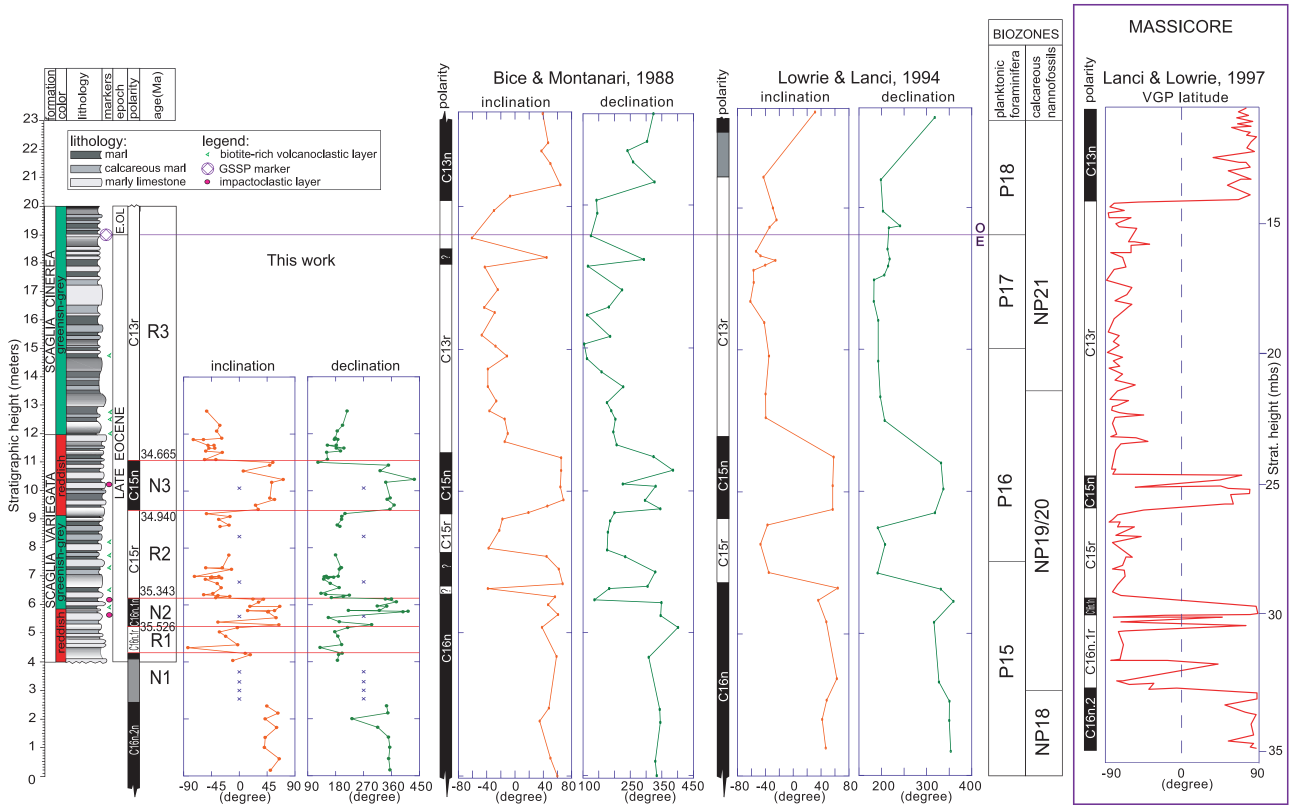

Figure 1. Lithostratigraphic column for the interval between 4 and 20 m, stratigraphic variation in the ChRM inclination and declination (this study), ChRM inclination and declination by *Lowrie and Lanci* [1994] and by *Bice and Montanari* [1988]. VGP latitude from MASSICORE are also showed [*Lanci and Lowrie*, 1997]. In the magnetic polarity zonation black (white) represents normal (reversed) polarity intervals. Numerical ages are from *Cande and Kent* [1995] (modified from *Jovane et al.* [2004]).

of several researchers, who sought to understand the role of these events on the evolution of the Earth's climate at the Eocene-Oligocene boundary.

[13] First, *Dall'Antonia et al.* [2002] and then *Coccioni and Galeotti* [2003] used the faunal and geochemical records to produce a detailed reconstruction of the paleoceanography and climate of the central Tethys region at the E/O boundary. Although strongly anchored to the problem of the impactoclastic events as a driver of climate evolution, the work of *Bodiselitsch et al.* [2004] provided a new high-resolution bulk-carbonate isotope record (samples spaced every 1 to 10 cm) from the Massignano section. Nevertheless, the "bulk-sample" approach, due to the generally imponderable contribution of diagenesis and multiple sediment sources, reduces the reliability of the isotope record as proxies of environmental condition and limits their use for qualitative interpretation. Conversely, isotope data from carbonates of selected organisms, specifically those living on the bottom sediments, are generally considered to provide more direct information on the evolution of deep waters and 3-D ocean circulation.

4. Methods and Materials

4.1. Sampling

[14] Before sampling, a bed-by-bed lithological log was constructed during several field trips (Figure 1). From 4 up to 20 msl, we cleaned the outcrop surface in order to remove the effects of surface weathering, and then collected 304 small unoriented block samples with an average spacing of 5 cm. In addition, 82 oriented samples were collected for magnetostratigraphy analysis on the most indurated marl or limestone beds in the proximity of the chron boundaries from 0 to 13 msl (mostly every 15 cm). We were not able to collect oriented samples above 13 msl because the lithology was not suitable (fractures, unconsolidated). We cut all 386 samples into multiple ~8 cm^3 cubic specimens and added a letter suffix (A, B and C) to their sample names. The weight of each sample was determined for subsequent mass normalization of magnetic properties.

4.2. Magnetostratigraphy

[15] Paleomagnetic measurements were carried out at the paleomagnetic laboratory of the Istituto Nazionale di Geofisica e Vulcanologia (INGV), Rome. We demagnetized the "A" specimens by stepwise heating (100, 200, 300, 330, 360, 400, 450, 500, 550, 600, 650, 700°C) and the "B" specimens by stepwise AF demagnetization in 12 steps (5, 10, 15, 20, 25, 30, 40, 50, 60, 80, 100 milliTesla, mT). Natural remanent magnetizations (NRM) were measured using an automated pass-through 2G Enterprises cryogenic magnetometer (model 750 R) with internal diameter of 4.2 cm, equipped with three DC SQUID sensors (noise level 3×10^{-9} A m^2 kg^{-1}). After each thermal demagnetization step, we monitored the low-field susceptibility in order to detect any thermally induced rock magnetic variation. The ChRM directions were

determined from interpretation of orthogonal diagrams [*Kirschvink*, 1980] and use of principal component analysis [*Zijderveld*, 1967]. Mean paleomagnetic directions were corrected for the structural tilt of the Massignano section, which tilts 21° degrees to the NW (strike N318°W).

4.3. Rock Magnetic Properties

[16] The magnetic properties were studied on the B specimens in order to obtain a quantitative inference of the variation in the composition, concentration and grain-size of magnetic minerals throughout the section. We built upon the previous investigation of *Jovane et al.* [2004], which presented high- and low-field susceptibilities, artificial remanences and calcium carbonate content profiles. The combined observations consist of the susceptibility (χ), the NRM, the anhysteretic remanent magnetization (ARM), the IRM at 900 mT (IRM@900) and backfield isothermal remanent magnetization (BIRM) at 100 mT (BIRM@100) and 300 mT (BIRM@300). From these measurements, we calculated S-ratios and hard isothermal remanent magnetizations (HIRM), both of which provided information about the magnetic coercivity of the magnetic carriers (see *Stoner et al.* [1996] for definitions of the various parameters).

[17] Low-field magnetic susceptibility measurements were made in laboratory using a KLY 2 (AGICO) Kappabridge with operating frequency of 920 Hz, magnetic induction of 0.4 mT (noise level 2×10^{-10} m^3 kg^{-1}). In addition, we measured hysteresis properties on 161 selected samples and first-order reversal curves (FORC) on 31 samples. In order to assess how compositional variations might correlate with magnetic properties, *Jovane et al.* [2004] determined calcium carbonate content on all samples. Saturation magnetization (M_s), saturation remanence (M_{rs}), and coercive force (B_c) were determined from hysteresis loops, and the back field measurements on the Molspin vibrating sample magnetometer (VSM) yielded values of remanent coercivity (B_{cr}). The gradient dM/dB from the aforementioned properties gives out the high-field susceptibility (χ_h) that reflects the paramagnetic minerals content. FORC measurements were made using an alternating gradient magnetometer (MicroMag Model 2900, with noise level of 2×10^{-10} Am^2) at the University of California, Davis. FORC analyses were conducted on the intervals most representative and with sufficiently strong magnetizations in order to investigate micro-coercivity and magnetic interaction among magnetic particles. The FORC diagrams were created using the FORCIT software [*Acton et al.*, 2007]. The saturation field for the IRM was 0.9T, which corresponds to the peak field used for hysteresis loops to define the M_{rs}. Indirect parameters, like S-ratios (S300 = BIRM@300/IRM@900 and S100 = BIRM@100/IRM@900) and HIRMs (HIRM300 = (IRM@900 + BIRM@300)/2 and HIRM100 = (IRM@900 + BIRM@100)/2), have been established in order to investigate the coercivity of the magnetic minerals. Also the ratio between ARM and IRM has been used to determine magnetic grain-size (ARM/IRM@900) [e.g., *Opdyke and Channell*, 1996; *Venuti et al.*, 2007]. We also investigated dependence of magnetic susceptibility up to a maximum temperature of 700°C on selected samples, measured with a furnace (CS3) equipped Kappabridge KLY 3 (noise level 2×10^{-8} SI), following the procedure described in *Hrouda* [1994]. For the same specimens we studied IRM acquisition and the stepwise thermal demagnetization of three orthogonal IRM components [*Lowrie*, 1990]. Fields of 1.2, 0.7, and 0.2 Tesla (T) were applied along the x, y, and z axes of samples to distinguish between high-, intermediate-, and low-coercivity magnetic phases, respectively.

4.4. Stable Isotopes

[18] Eighty-six stable isotope analyses were carried out on 2–3 aragonitic valves of the Agrenocythere ostracod genera. They were measured by an automated continuous flow carbonate preparation GasBenchII device [*Spötl and Vennemann*, 2003] and a ThermoElectron Delta Plus XP mass spectrometer at the IAMC-CNR (Naples) geochemistry laboratory. Intense ultrasonic washing in Millipore water was carried out to clean samples from secondary carbonate encrustations and clay matrix, then the samples were baked at 430°C in a vacuum. Acidification of samples was performed at 50°C. For a typical run with 30 samples, every sixth sample was an internal standard (Carrara Marble with $\delta^{18}O = -2.43‰$ vs. VPDB and $\delta^{13}C = 2.43‰$ vs. VPDB) and, for each run, the NBS19 international standard was measured. Standard deviations of carbon and oxygen isotope measures were estimated 0.1 and 0.08‰, respectively, on the basis of $\sim$10 repeated samples. All the isotope data are reported in per mil (‰) relative to the VPDB standard.

4.5. Principal Component Analysis and Fuzzy *c*-mean Cluster Analysis

[19] We used principal component analysis (PCA) [*Gonzalez and Woods*, 1992] to find the number of uncorrelated parameters from seven possible correlated parameters (low field susceptibility, ARM, IRM, HIRM300, S300, $CaCO_3$, ARM/IRM@900). High values in the PCA demonstrate similarity and correlation in the variable of the chosen parameters. We determined the PCA from the mean of the covariance of the transposed matrix of all the normalized parameters chosen using Matlab.

[20] We also used fuzzy *c*-means (FCM) cluster analysis, which is a multivariate statistical technique requiring no *a priori* knowledge, to designate groups (or clusters) with similar characteristics [*Hanesch et al.*, 2001]. This similarity is conveyed in a continuous function between zero (completely different) and one (identical) [*Dekkers et al.*, 1994]. The choice of the cluster number is selected by the user and is based on the number of groups or clusters of data occurring in the scattergrams (plots of one variable against another). We conducted FCM cluster analysis on the same parameters as used in the PCA.

5. Results

5.1. Magnetostratigraphy

[21] Most samples displayed stable paleomagnetic behavior upon stepwise thermal demagnetization (Figure 2). Demagnetization paths in orthogonal vector diagrams are generally sufficiently good to define a magnetic polarity zonation, although the paths are noisy enough that we would not recommend using the paleomagnetic directions for apparent polar wander, paleointensity or tectonic studies. The noisy NRM demagnetization paths are attributed to the relatively

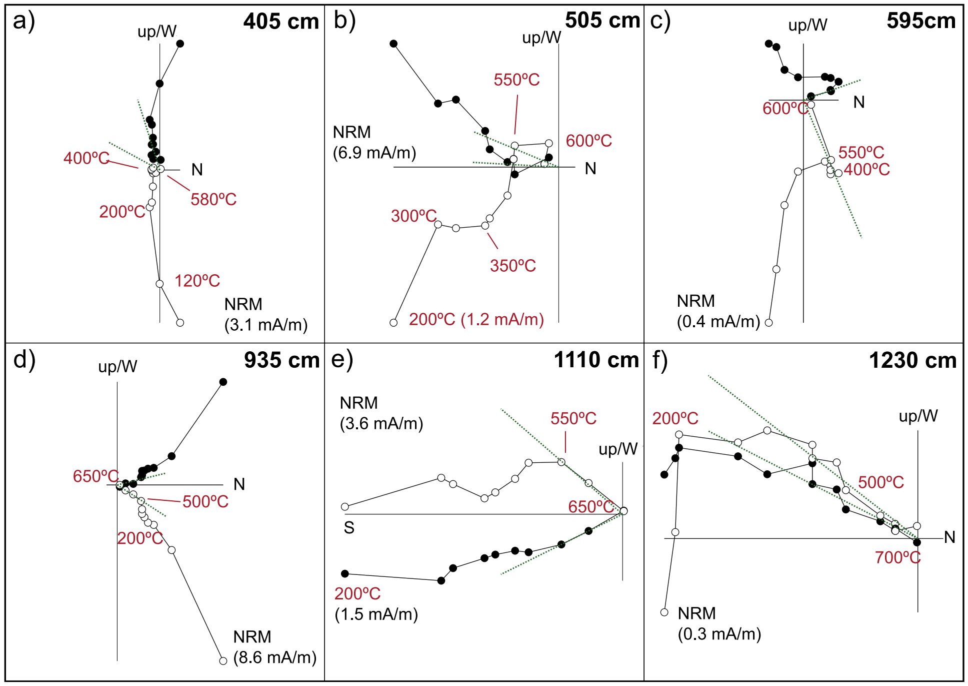

Figure 2. Bedding-corrected orthogonal plots of thermal demagnetization data from representative normal (c, d) and reverse (a, b, e, f) specimens. Solid (open) symbols represent projections onto the horizontal (vertical) plane. The fitted ChRM direction, the NRM intensity, the stratigraphic level in centimeters, and some step treatments are indicated for each example.

low intensity of magnetizations (1.5 to 6 $\times$ 10^{-6} Am^2/kg with a mean of 3 $\times$ 10^{-6} Am^2/kg). Only a few intervals are characterized by high NRMs and these are associated, among the others, with the impactoclastic and volcanoclastic layers. The overall long wavelength trend of NRM intensities follows the low-field susceptibility curve, indicating that the magnetic mineral concentration is key in controlling the NRM magnitude.

[22] AF demagnetization treatment was less effective than thermal demagnetization in removing secondary magnetization components and in isolating the ChRM components for both normal and reversal polarity samples. Based on visible inspection of the vector component diagrams, coherent paleomagnetic behavior was obtained for 93% of the thermally demagnetized samples whereas only 68% of the AF demagnetized samples were stable. Usually the ChRM was resolved with thermal demagnetization above 450°C (Figure 2). Reddish intervals required higher temperatures to remove secondary magnetizations due to the presence of high-coercivity magnetic minerals.

[23] The normal polarity samples have a mean inclination of 57.2° and declination of 349° (N = 27; α_{95} = 13.6) and the reverse polarity samples have a mean inclination of −39.6° and declination of 182.7° (N = 43; α_{95} = 7.1). The inverted mean reversed polarity direction differs significantly from the expected direction (Dec = 6°; Inc = 56°), although the mean normal polarity direction does not. Even within the rather large directional uncertainties, these results fail the reversal tests as the mean normal direction differs by 19.7° from the inverted mean reversed polarity. This most likely results from the generally noisy demagnetization behavior of these weakly magnetized sediments in conjunction with incomplete removal of secondary components. A small unremoved recent magnetic overprint would also explain the shallower than expected inclination for the reversed polarity samples.

[24] We divided the studied magnetic polarity record, which encompasses the Massignano section from 0 to 13 msl, into six main magnetozones (Figure 1). These magnetozones are defined as intervals with multiple, consecutive samples with polarities that are distinctly different from neighboring intervals. A few samples have opposite polarities to those of the rest of the magnetozone in which they reside. The first 4.15 msl of the section are dominantly normal polarity (magnetozone N1). Above this magnetozone, there are 7 samples from 4.15 to 5.20 msl with reverse polarity (R1). The Magnetozone N2 spans from 5.20 to 6.22 msl, magnetozone R2 spans from 6.22 to 9.27 msl, magnetozone N3 from 9.27 to 11.05 msl, and magnetozone R3 spans from 11.05 msl to the top of the studied section.

[25] The new magnetozones correspond well to the previous magnetostratigraphies on Massignano [*Bice and Montanari*, 1988; *Lowrie and Lanci*, 1994; *Lanci and Lowrie*, 1997]. The higher resolution of this study allowed us to refine the position of polarity boundaries and to identify new chronozones within the section (Figure 1).

[26] We interpreted the magnetozones based on the GPTS [*Cande and Kent*, 1995], where N1, R1, N2, R2, N3 and R3 correspond respectively to Chron 16n.2n, 16n.1r, 16n.1n, 15r, 15n, and 13r (Figure 1). The few reversed samples in the N1 could be related to the C16n.1r. Unfortunately, the 4 samples with uncertain polarity that occur around 3 msl make it difficult to define accurately the boundary between Chrons C16n.2n and C16n.1r.

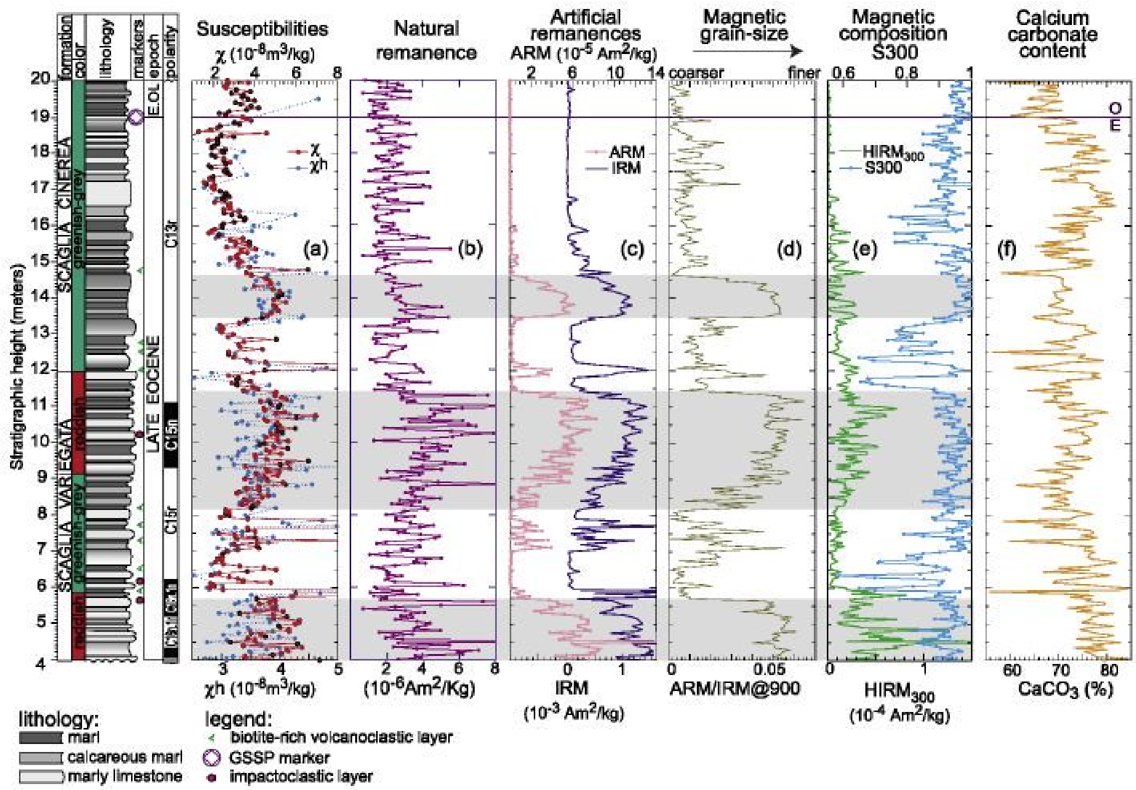

Figure 3. Lithostratigraphic column for the interval between 4 and 20 m at Massignano stratotype section and mineral magnetic parameters as a function of stratigraphic position. (a) low-field magnetic susceptibility (χ) and high-field (χh) (paramagnetic) susceptibility; (b) natural remanent magnetization; (c) isothermal remanent magnetization and anhysteretic remanent magnetization; (d) ARM/IRM@900: increasing values of this ratio indicate relatively higher concentrations of finer particles; (e) HIRM300 (HIRM300 = (IRM@900 + BIRM@300)/2); (f) S-ratio$_{300}$ (S300 = BIRM@300/IRM@900); (f) $CaCO_3$ (%) content. The shaded areas mark the intervals with high concentrations of magnetic minerals (modified from *Jovane et al.* [2004]).

5.2. Environmental Magnetism

5.2.1. Magnetic Properties

[27] The records, from 4 to 20 msl, of the low-field magnetic susceptibilities (Figure 3a) (mean of 4×10^{-8} m^3/kg), ARM (Figure 3c) (mean of 2×10^{-5} Am^2/kg), IRM (Figure 3c) (mean of 5×10^{-4} Am^2/kg), and a magnetic grain-size proxy ARM/IRM@900 (Figure 3d) (bimodal distribution with modes of 0.013 and 0.048) follow the same alternating high (finer) and low (coarser) magnetic mineral concentration trend, which has no apparent relationship to the main lithostratigraphic features [*Jovane et al.*, 2004]. Parameters sensitive to coercivity variations, like H_c (Figure 4b) and HIRMs (Figure 3e) (mean of 1.6×10^{-5} Am^2/kg) demonstrate the predominance of low coercivity magnetic minerals in the intervals with low magnetic mineral concentration [*Jovane et al.*, 2004]. In contrast, the intervals with high magnetic mineral concentration have a mixture of low and high coercivity minerals. The FORC diagrams indicate that the presence of low coercivity magnetic minerals is higher in concentration in the levels that correspond to the biotite-rich volcanoclastic and iridium impactoclastic layers than the surrounding intervals (Figure 6). It seems that the concentration of a low magnetic coercivity mineral (interpreted to be magnetite) increases in these layers (Figure 3). The S300 also (Figure 3e), retaining median values of 0.91, indicate that the magnetic mineralogy is a complex mixture of high and low coercivity components within these layers.

[28] Hysteresis parameters (Figure 4), HIRM300 record, thermal demagnetization of a composite 3-axis IRM (Figure 5), IRM acquisition curves (Figure 5), thermomagnetic curves (Figure 5) and FORC diagrams (Figure 6) indicate a variable mixture of low and, secondarily, high coercivity components in the lower part of the section (Scaglia Variegata Formation) and a magnetic mineral composition that has mostly low coercivities in the upper half of the section (Scaglia Cinerea Formation). We interpret these results to indicate that magnetite is the dominant magnetic mineral, but that goethite, maghemite and hematite are also present in some intervals. From the analyses of the thermomagnetic runs, the presence of goethite is inferred from the smooth step at ^120°C (Figure 5c) while maghemite may be inferred from the increase of susceptibility at ^300°C, at which point maghemite can transform into magnetite and hematite with further heating. Alternatively, the increase may be totally due to the Hopkinson peak for magnetite, which is a peak in susceptibility that occurs at temperatures just below the Curie temperature [*Hopkinson*, 1889]. As it is evident from the thermomag-

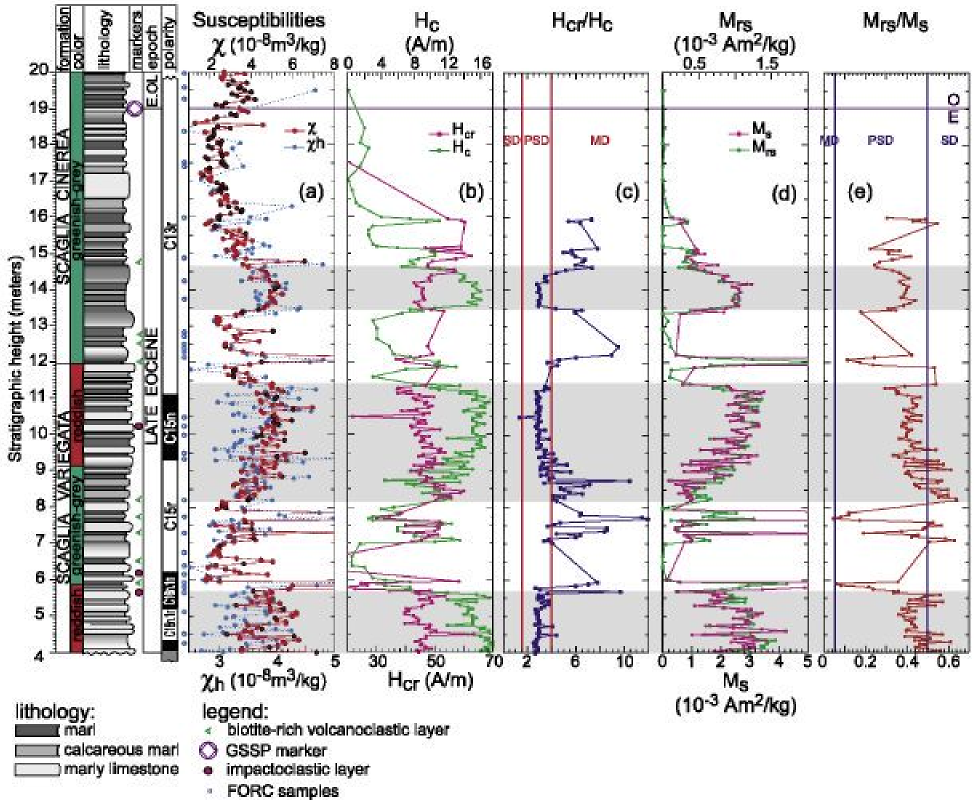

Figure 4. Lithostratigraphic column for the interval between 4 and 20 m at Massignano stratotype section and mineral magnetic parameters as a function of stratigraphic position. (a) low-field magnetic susceptibility (χ) and high-field (χh) (paramagnetic) susceptibility; (b) coercive force (H_c); (c) remanent coercivity (H_{cr}); (d) H_{cr}/H_c and redlines that delimits magnetite magnetic domain structures; (e) saturation magnetization (M_s); (f) saturation remanence (M_{rs}); (g) M_{rs}/M_s and blue lines confining domain states for magnetite. For most of the samples above ca. 16 msl, the graphs are extremely noisy and this hampered attempts to define valid estimates for H_{cr} and M_s. The shaded areas mark the intervals with high concentrations of magnetic minerals (modified from *Jovane et al.* [2004]).

netic curve, the dominant magnetic mineral has a Curie temperature of about 560-580°C, consistent with the presence of magnetite.

[29] These rock-magnetic analyses [see also *Jovane et ah*, 2004, 2006] are comparable with those obtained in *Lowrie and Land* [1994] and *Land and Lowrie* [1997], who interpret magnetite to be the main magnetic mineral for the Scaglia Cinerea Formation samples and a mixture of magnetite and hematite to be the main magnetic minerals in the Scaglia Variegata Formation. Generally in the Scaglia Cinerea Formation there is a low concentration of high coercivity minerals, except for its lower part where the hematite contribution is scanty. On the contrary, in the Scaglia Variegata Formation, a complex mixture of magnetite, maghemite, hematite and trace of goethite are found in the magnetic assemblage.

[30] The FORC diagrams illustrate that nearly all samples have coercivities distributions that fall dominantly between 0 and 60 mT. Significant differences, however, do exist between those samples that have negligible concentrations of magnetic grains with coercivities higher than about 60 mT (samples from 5.8, 12.15, and 12.8 msl in Figure 6) and those that have substantial high coercivity concentrations (all other samples in Figure 6). All those samples with substantial coercivity distributions >60 mT, fall within the shaded regions in the stratigraphic plots (Figures 3 and 4).

[31] Calcium carbonate content analysis from *Jovane et al.* [2004] (Figure 3f) give a mean value of 73%, with little variations over the entire section. The tiny fluctuation of bulk weight percent carbonate (%$CaCO_3$) indicates that no obvious relationship exists between the calcium carbonate content and the long-term intervals with contrasting magnetic properties. In detail, there is a small correlation between the high and low magnetic mineral concentration zones and the $CaCO_3$ profile, but there is also a more evident opposite relation (anti-correlation) in the higher frequencies. This is most evident for the low-field susceptibility or the S300 ratio, where higher values correspond to lower calcium carbonate content.

5.2.2. Scattergrams, PCA and FCM Cluster Analysis

[32] Scatter diagrams (Figure 7) are used to discriminate between distinct environmental conditions. Susceptibility is compared with %$CaCO_3$, IRM with ARM/IRM@900 (as concentration against grain size relationship), IRM with HIRM (representing the concentration divided composition parameter) and finally HIRM with ARM/IRM@900 (for composition and grain-size comparison). In all the scattergrams, two dominant groups can be distinguished. One

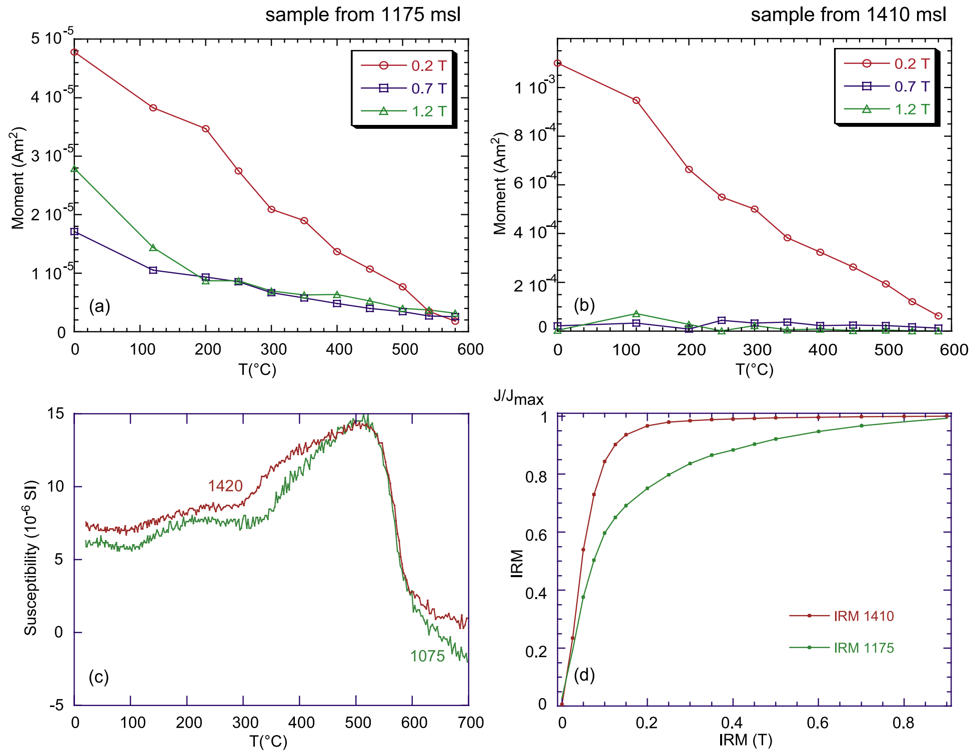

Figure 5. Thermal demagnetization of a composite IRM (a, b) (IRM acquisition of three orthogonal IRM components in successively, 1.2, 0.7 and 0.2 T and stepwise thermal demagnetization [*Lowrie*, 1990]); we present a temperature dependence of magnetic susceptibility up to a maximum temperature of 700°C (c) and stepwise acquisition of IRM up to 0.9 T (d) for representative samples from both Scaglia Variegata (red in c and d) and Scaglia Cinerea Formations (green in c and d). Three-axis method shows how Scaglia Variegata (a) samples keep the magnetization in the stronger components during the thermal demagnetization signifying the presence of high coercivity minerals on the contrary of b. The same pattern is demonstrated from the thermomagnetic curves, which also illustrate that above 300°C new magnetite is being created (c). Acquisition curves of the IRM (d) illustrate the coercivity spectrum.

group is characterized by high magnetic mineral concentration, finer grain size, and higher coercivities, which are associated with compositions that are mainly magnetite with some hematite. The other group is characterized by low magnetic mineral concentration, coarser grain sizes, and lower coercivities, which are associated with magnetic compositions that are completely dominated by pseudo-single domain (PSD) to multidomain (MD) magnetite.

[33] The variations in the PCA covariance agree well with the FCM cluster analysis (Figure 8), with high covariance occurring for the intervals with low magnetic mineral concentration, larger grain size, and lower coercivity and low covariance occurring for intervals with high concentration, smaller grain size, and higher coercivity (see the shaded intervals in Figure 8). The FCM cluster analysis is more clearly bimodal than the PCA covariance analysis, although both methods do resolve the bimodality of the rock magnetic properties. The lower covariance for the high magnetic concentration intervals indicates that the variability between rock magnetic parameters is greater for the low magnetic concentration intervals, which is also apparent in the scattergrams (Figure 7). The negative values in the PCA for single sample at 4.50 msl is due to the uniquely large ARM of this sample, which is probably indicative of a large concentration of fine-grained magnetite in this sample.

[34] We suggest that the bimodal nature of our climatic data set as evidenced by both cluster analyses, depends upon an on and off switching process. This process represents two different alternating paleoceanographic conditions in the basin, affecting all climatic proxies contemporaneously.

5.3. Stable Isotopes

[35] The picked ostracod valves from the Massignano Section are moderately well-preserved. They generally have some encrusted irremovable matrix and, more rarely, some blocky calcite. Although it is not possible to exclude *a priori* the influence of diagenesis on the isotope composition of the studied ostracod specimens, an accurate selection of the best preserved valves, the absence of covariance between $\delta^{18}O$ and $\delta^{13}C$ signals, and the heavy cleaning approach preceding the isotope measurements, make us confident that the records can be reliably used as proxies of the paleoceanographic conditions that characterized the Massignano basin during the studied interval.

[36] The $\delta^{13}C$ values (Figure 9) range between +0.12‰ and +1.43‰; values increase from the base of the section (averages of ~0.80‰) peaking at about 6 msl (1.42‰). Then, a progressive negative excursion shifts the $\delta^{13}C$ values to a minimum of 0.12‰ at 16.2 msl. From there, a positive excursion up to the top of the section shifts the $\delta^{13}C$

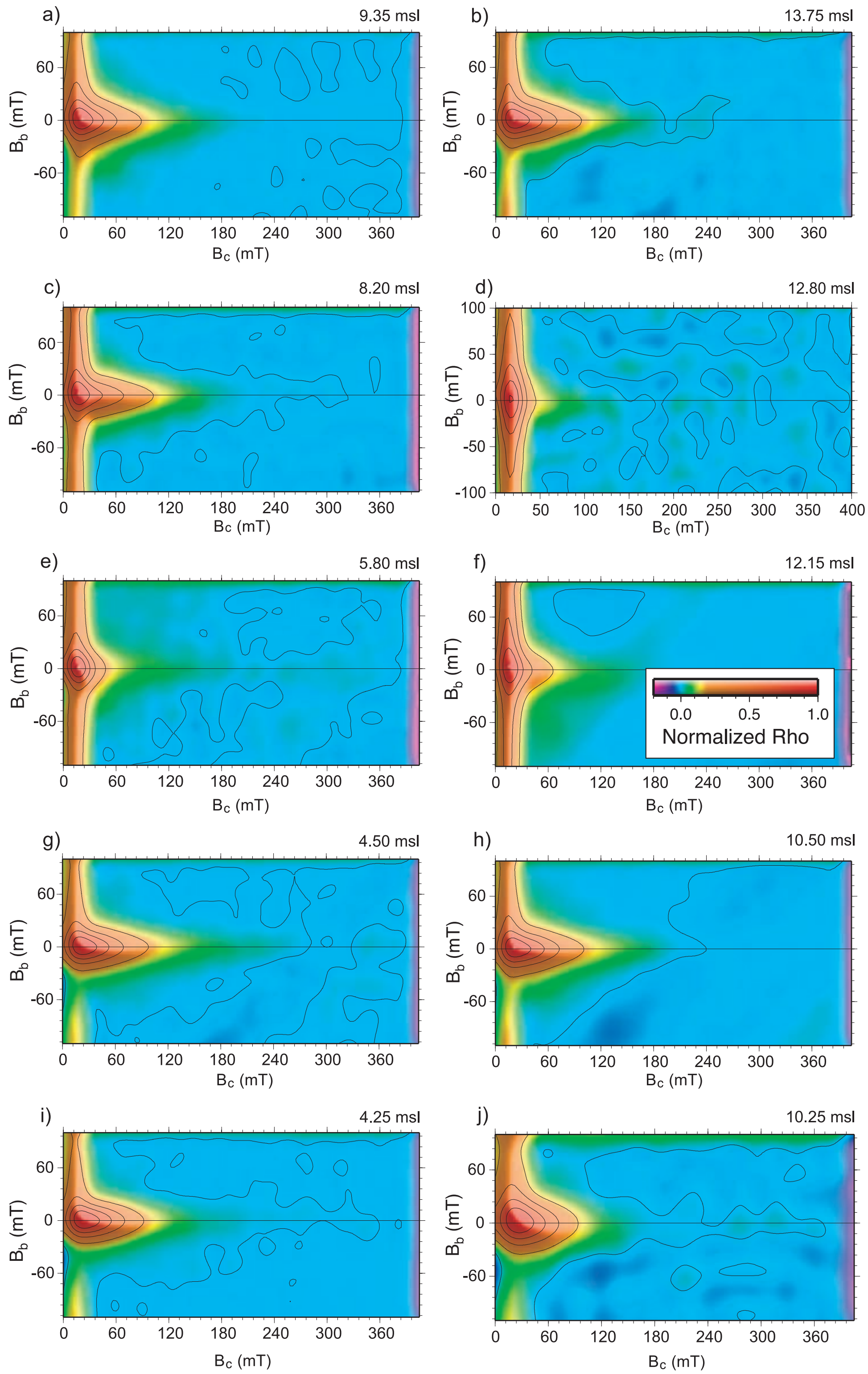

Figure 6. Representative FORC diagram (Gaussian filter of 7.2 mT except for 10.25 and 12.80 msl that is 9.6 mT and 7.8 mT respectively) for samples from different stratigraphic levels (given in msl on the plot). The dominant peak near the origin for the samples in panels (a), (b), (g), (h), and (i) corresponds to interval with high magnetic properties, which is consistent with the presence of magnetite, while the small peak at B_c = 200–250 mT indicates the presence of a high coercivity mineral (e.g., hematite). Panels (c), (d), (e), (f), and (j) are for samples collected from impactoclastic and volcanoclastic layers respectively, shows higher peaks near the origin due to lower presence of high coercivity mineral.

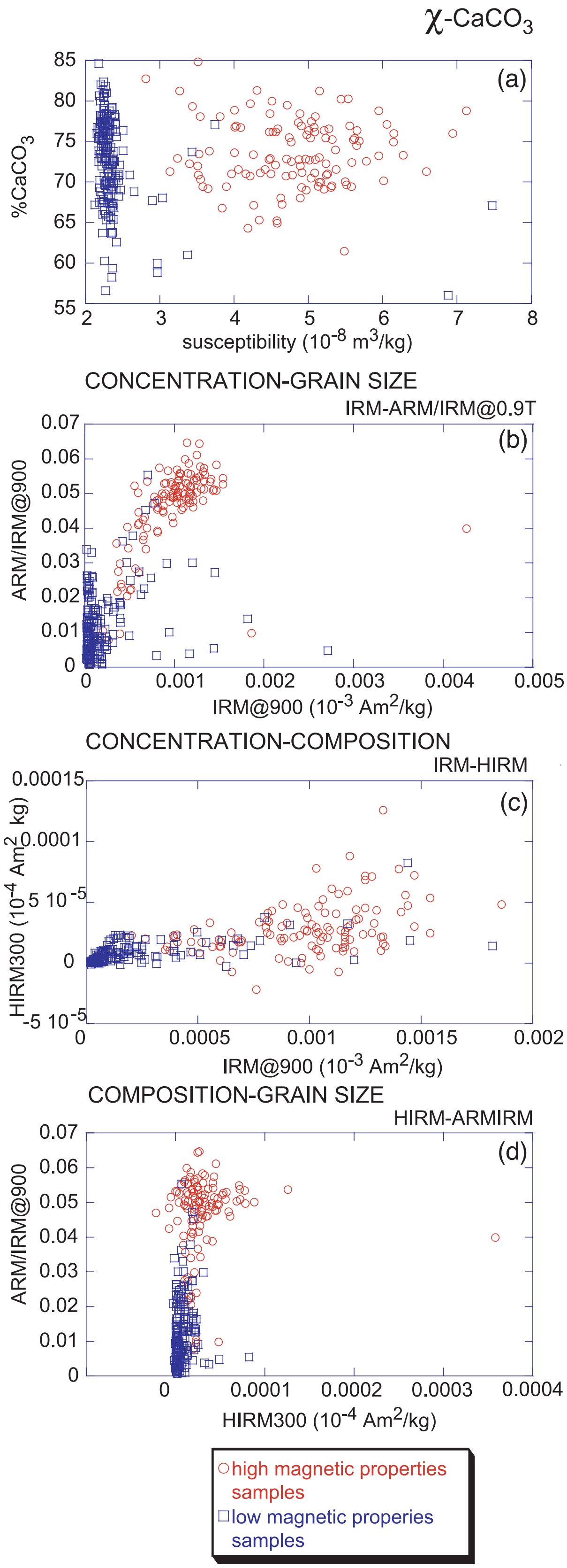

values to averages of about 0.90‰. Superimposed on this long-term trend are shorter wavelength negative excursions that occur in the intervals from 1.8 to 3.9 msl (averages of 0.90‰), from 6.2 to 7.1 msl (average 0.90‰), from 8 to 9.3 msl (averages of 0.70‰), from 10.7 to 12.3 msl (average 0.40‰), from 15.5 to 16.7 msl (average 0.30‰) and from 18.9 to 20.7 msl (average 0.50‰). The $\delta^{18}O$ values (Figure 9) range between -1.64‰ and $+0.87$‰; values progressively decrease from the base of the section to 6 msl (-1.60‰). Above this, an abrupt positive excursion occurs, which reaches a maximum of 0.68‰ at 7.7 msl. Then, superimposed on a long negative trend up to 16.8 msl (-0.87‰), two abrupt spikes shift the oxygen isotope composition to very low values (-1.63 and -1.22‰) at 9.5 and 10.4 msl, respectively. A final positive excursion was recorded from 16.8 msl to the top of the section.

[37] Direct comparison of our isotope data set with that of *Bodiselitsch et al.* [2004] reveals similar $\delta^{13}C$ trends, although with numerical values $\sim$1‰ lower than those measured in the bulk samples. In contrast, oxygen isotopes from bulk-samples are very noisy, while the $\delta^{18}O$ signal from ostracods shows a highly structured signal with high frequency oscillations superimposed on longer-term trends. Since the $\delta^{18}O$ and $\delta^{13}C$ offsets between isotope composition of the carbonate in the ostracods relative to that in the seawater are unknown for the selected genera, our interpretation of isotope results is limited to their relative variations.

6. Paleoceanography Discussions at the Eocene-Oligocene Boundary

6.1. Discussion on the Environmental Magnetism

[38] One of our primary observations is that only the environmental magnetic record provides evidence of the long-term bimodal variations in sedimentation. In contrast, short-term variations are apparent in the lithology, susceptibility, and calcium carbonate content and recently have been shown to have orbital periodicities (obliquity and 100-k.y. eccentricity) [*Jovane et al.*, 2006]. The origin of short-term variations appears to be related to global oceanographic and climatic changes [*Wade and Pälike*, 2004; *Coxall et al.*, 2005]. The atypical bimodal distribution of the high and low magnetic properties fluctuation appears to be controlled by a process that switches on and off. The time to switch between these opposite phases is abrupt, being virtually geologically instantaneous within the resolution of the sedimentary record. Likewise, it seems natural that the bimodal signal is also controlled by longer-term oceanographic and climatic changes, or perhaps by regional tectonics that influence the sea currents.

[39] We maintain that the presence, abundance, and composition of the magnetic minerals are related to paleo-

Figure 7. Scattergrams showing the comparison between the magnetic susceptibility and calcium carbonate content (a), and between composition, concentration and magnetic grain-size parameters (b, c, d) subdivided in high magnetic properties minerals and low magnetic properties minerals in relation to the bands of Figures 3 and 4. That plots permits to define the number of cluster to run the FCM cluster analysis.

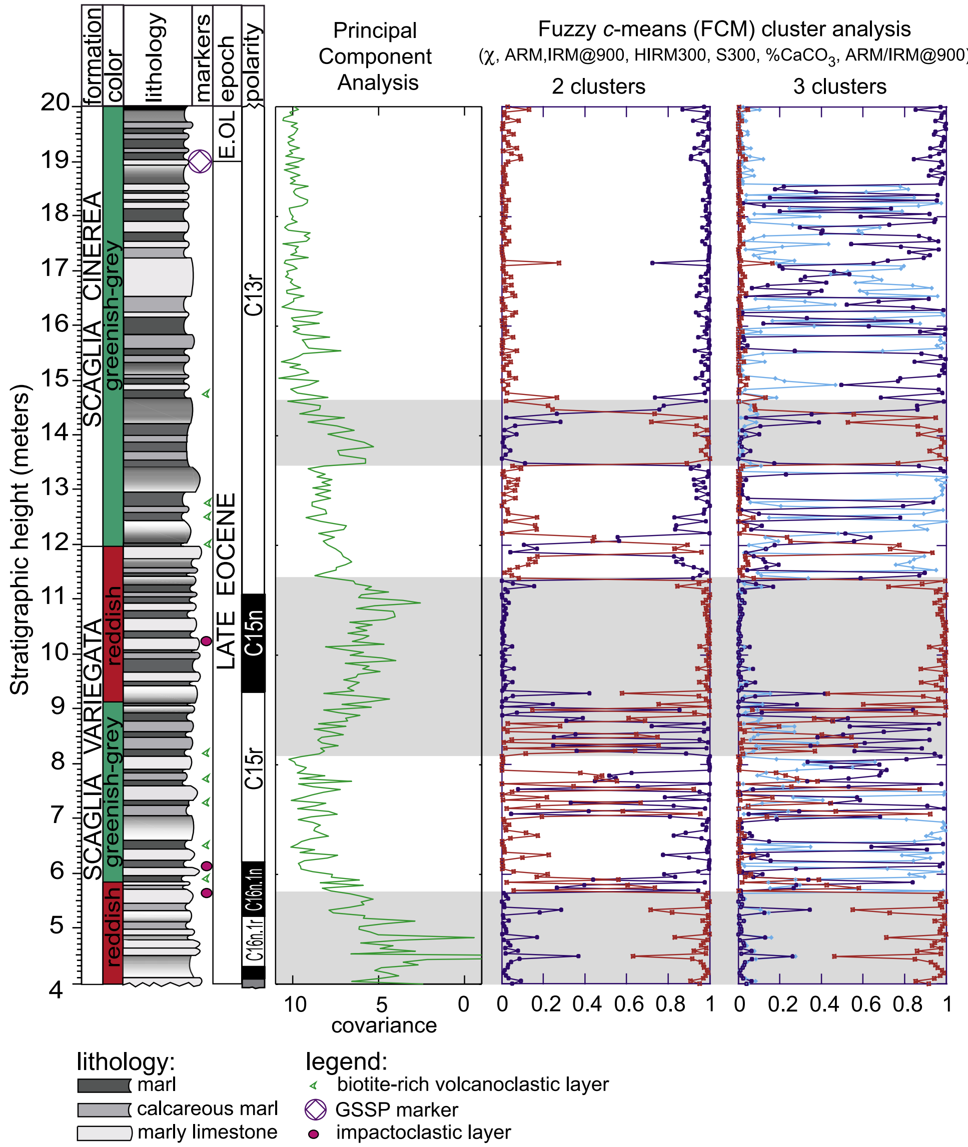

Figure 8. Vertical distribution along the section of PCA for variables and the centers values for the 2 clusters and 3 clusters interpretation: susceptibility, ARM, IRM, HIRM300, S300, $CaCO_3$, ARM/IRM@900. Those implements show statistically the atypical bimodal distribution (2 cluster) along the section and the similarities for the different variables in our Massignano data set. The third cluster just follows the two distributions except for the last 5 m where it inverts the path, meaning, may be, a degradation of the previous switching distribution.

ceanographic changes that occurred in the deep-sea environment as a coupling and/or alternation of detrital and biological origin. Other short-term events, such as the volcanoclastic and impactoclastic events, also caused enrichment of ferromagnetic and paramagnetic minerals in the basin, but these events are unrelated to the dominant bimodal magnetic signal. Fluctuations between the low and high magnetic mineral concentrations may be related to changes in flux (biogenic vs. terrigenous), sediment sources, and/or sediment transport processes ultimately driven by paleo-current changes that may be linked to climatic, tectonic, or sea level changes.

[40] Clay minerals [*Mattias et al.*, 1992] are dominated by smectite, which remains constant along the section indicating homogeneous chemical weathering conditions of source rocks, with a small increase of illite in the upper part. The consistency of the clay mineralogy assemblages indicates that the amount and composition of the terrigenous material derived from nearby continental regions did not vary significantly. We interpret this to indicate that climatic variations on the continent and changes in continental runoff were relatively minor.

[41] Thus, our preferred interpretation is that the influx of magnetic materials is controlled by paleo-current variations. Those variations could be related to the closing of the gateway between Indo-Pacific Ocean and Atlantic Ocean, which would have upset the transport of sediments and nutrients. As the gateway progressively closed over time, flow through it possibly fluctuated between being dominantly on or off, thus producing the bimodal rock-magnetic

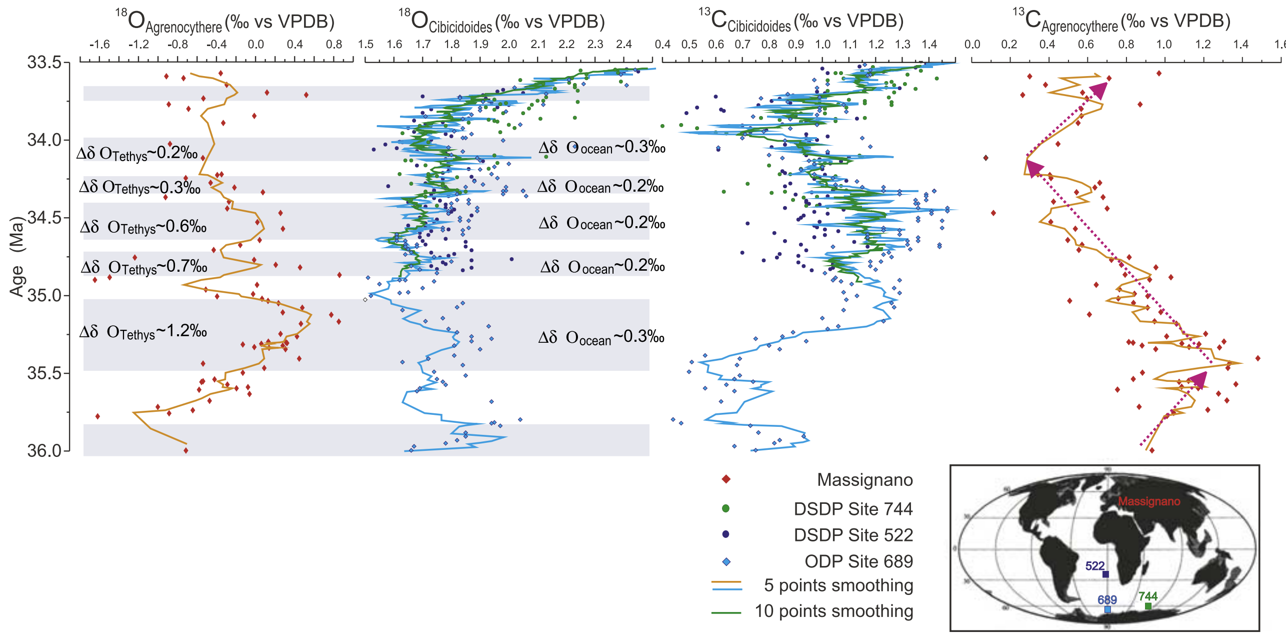

Figure 9. Comparison of (a) δ^{18}O and (d) δ^{13}C isotope record measured on valves of the Agrenocythere ostracod genera throughout the Massignano section and (b) δ^{18}O and (c) δ^{13}C isotope record measured on *Cibicidoides* from DSDP Site 522 (Angola Basin), Site 744 (southern Indian Ocean) from *Zachos et al.* [1996] and from ODP Site 689 (Maud Rise, Weddell Sea) from *Diester-Haass and Zahn* [1996]. The shaded areas mark the intervals with parallel variation in $\Delta\delta^{18}$O.

signature observed at Massignano. Possibly sea level changes and/or tectonics had a direct role in turning the currents on and off.

[42] Variations in sea-bottom ventilation and productivity have been described in previous works on Massignano [*Coccioni et al.*, 2000; *Dall'Antonia et al.*, 2002; *Coccioni and Galeotti*, 2003] and on the Umbria-Marche Basin [*Verducci and Nocchi*, 2004] for this period. These variations have been interpreted as arising from changes in the paleoceanographic conditions of the Neo-Tethys [*Dercourt et al.*, 2000] during the late Eocene and early Oligocene.

[43] The relationships between magnetic properties fluctuations [e.g., *Jovane et al.*, 2004], productivity [*Coccioni and Galeotti*, 2003], paleoceanographic variations [*Coccioni et al.*, 2000; *Dall'Antonia et al.*, 2002; *Coccioni and Galeotti*, 2003; *Verducci and Nocchi*, 2004], and red beds [*Hu et al.*, 2005; *Jovane et al.*, 2007] in the Umbria-Marche Basin are still far from being resolved. Further petrographical, biostratigraphical and magnetic analyses are needed in the Neo-Tethys region to clarify if the observations at Massignano are of local, regional, or of global significance. With the data obtained at the Massignano section so far, we are only able to hypothesize that some bimodal process related to the paleoceanographic conditions affects the Neo-Tethys.

6.2. Discussion on Stable Isotopes

[44] A complex history of the bottom water evolution in the basin where Massignano's sediment deposited during the ~3.0 m.y. preceding the E/O boundary emerges from the stable isotope data. A direct comparison of our isotope data set with high-resolution benthic isotope records (all collected on the benthic foraminifer genera *Cibicidoides*) from DSDP Site 522 (Angola Basin), Site 744 (southern Indian Ocean) from *Zachos et al.* [1996], and from ODP Site 689 (Maud Rise, Weddell Sea) from *Diester-Haass and Zahn* [1996] is illustrated in Figure 9. The age model for the marine sites is based on the GPTS of *Cande and Kent* [1995]. The estimated age differences between the *Gradstein et al.* [2004] and *Cande and Kent* [1995] for the chron boundaries recognized throughout the studied intervals are irrelevant and lower than 20 k.y. [see *Jovane et al.*, 2006]. The isotope record from the Massignano section has lower resolution than the composite marine record and some age offsets may occur between the records. In particular, the resolution at the base of the Massignano record (from 36.0 and 35.6 Ma) and at its top (from 33.8 and 34.3 Ma) is poor and makes the proposed correlations with the marine record difficult and an accurate estimation of the $\Delta\delta^{18}$O amplitude uncertain.

[45] The oxygen isotope variations from the Massignano record and the marine record correlate in some intervals (evidenced by the grey bands in Figure 9) although significant differences also exist. The estimated $\Delta\delta^{18}$O of the complete isotope excursions from the Massignano section are generally larger than that measured for the marine sections and the main shift at the top of the marine record is not recorded at Massignano. This may suggest that some short-term global cooling/warming events were recorded in the Tethyan region by variations in sea surface temperature. However, a positive shift in the evaporation/precipitation (E-P) budget (with associated enhanced positive excursion in the δ^{18}O signal) could be amplified at regional scale by global climate forcing.

[46] Comparison among carbon isotope records from the Tethyan area and the global ocean appears more complex. Carbon isotopes generally provide key information about

Table 1. List of Bio-Chrono-Magnetostratigraphic Events Aged With the New Age Model Established on the Base of the New Magnetostratigraphy and the Astronomical Calibration [*Jovane et al.*, 2006], Compared to the GTS [*Gradstein et al.*, 2004; *Berggren et al.*, 1995][a]

Event	Level, m	Age From Magnetostratigraphy and Astronomical Tuning [*Jovane et al.*, 2006], m.y.	Age From GTS [*Gradstein et al.*, 2004; *Berggren et al.*, 1995], m.y.
FO *I. recurvus* [*Coccioni et al.*, 1988]	3	35.900*	36.0
LO *T. pomeroli* and LO *G. semiinvoluta* [*Spezzaferri et al.*, 2002]	4.8	35.520	35.3
Base Cr16n.1n (this work)	5.2	35.472	35.526
FO *C. oamaruensis* [*Monechi et al.*, 2000]	5.7	35.404	35.4
Top Cr16n.1n (this work)	6.22	35.340	35.343
FO *T. cunialensis* [*Spezzaferri et al.*, 2002]	7.5	35.185	35.0/36.1
LO *R. reticulata* (ex *C. reticulatum*) [*Monechi et al.*, 2000]	7.9	35.138	35.2
Base Cr15n (this work)	9.27	34.960	34.94
Top Cr15n (this work)	11.05	34.728	34.655
LO *G. index* [*Coccioni et al.*, 1988]	13.5	34.400	34.3
K-Ar and ^{40}Ar-^{39}Ar [*Premoli Silva et al.*, 1988]	14.7	34.254	34.3
LO *C. inflata* [*Coccioni et al.*, 1988]	15	34.221	34.0
E/O – LO *Hantkenina* spp. [*Premoli Silva et al.*, 1988]	19	33.703	33.9
Base Cr13n [*Lowrie and Lanci*, 1994]	21.5	33.545*	33.545

[a]The symbol * means that the values are defined on the magnetostratigraphy alone, without the astronomical tuning. The astronomical tuning obtained by *Jovane et al.* [2006] for the Massignano section provides revised ages for the main bio-chrono-magnetostratigraphic events [*Bice and Montanari*, 1988; *Bodiselitsch et al.*, 2004; *Coccioni and Galeotti*, 2003; *Coccioni et al.*, 1988, 2000; *Lowrie and Lanci*, 1994; *Lanci et al.*, 1996, 1998; *Lanci and Lowrie*, 1997; *Monechi et al.*, 2000; *Montanari et al.*, 1988, 1993; *Odin et al.*, 1988; *Premoli Silva and Jenkins*, 1993; *Spezzaferri et al.*, 2002] recorded throughout the Massignano record.

variations in marine export production and rate of organic matter re-mineralization as well as evidence about the evolution of ocean bottom circulation and its residence time (aging) of the deep water. In particular, relative lightening of δ^{13}C values can be triggered by more significant re-mineralization processes of organic matter during periods of sluggish circulation and, conversely heavier δ^{13}C values related to intervals of more intense circulation.

[47] From 36.0 to 35.4 Ma, the oxygen and carbon isotope signals at Massignano show a synchronous positive excursion that, according to the hypothesis proposed by *Coccioni and Galeotti* [2003], may be related to the incursion of cooler oceanic water at the bottom of the central Tethyan basin inducing reinvigorated bottom circulation in the basin. In turn, the increasing δ^{18}O values suggest colder temperatures and/or positive shift in the E-P budget (when compared with the stratigraphically lower intervals) in the source areas of bottom water. The coeval δ^{13}C at ODP Site 689 show very low values interpreted by *Diester-Haass and Zahn* [1996] as direct indication of a low productivity regime in the southern ocean.

[48] From 35.4 Ma up to 34.1 Ma, δ^{13}C values in the Tethyan realm progressively decrease, indicating that bottom circulation was becoming progressively more sluggish. The coeval response of the ocean δ^{13}C signal shows an evident positive excursion generally associated to an increasing productivity that *Diester-Haass and Zahn* [1996] attributed to the opening events of the Drake Passage to intermediate depth that permitted cooling of surface waters and induced enhanced surface productivity. By about 34.3 Ma, the global δ^{13}C record begins to decrease similar to the continuing decrease of the Massignano record.

[49] The final δ^{13}C positive excursion measured from about 34.0 Ma up to the top of the Massignano section agrees well with the positive shift recorded in the global marine record and coincides with the beginning of the δ^{18}O positive excursion of the Oi-1 event. The associated cooling event [e.g., *Zachos et al.*, 1996] may have represented a trigger for increasing ocean fertility. The appearance of a continental-size ice sheet in Antarctica during the earliest Oligocene may have intensified thermohaline and atmospheric circulation and, consequently, resulted in higher rates of oceanic turnover [e.g., *Zachos et al.*, 1996 and reference therein] directly related to the steepened temperature gradient.

[50] In summary, the oxygen isotope record at Massignano documents some of the global cooling events, although this events are amplified at the regional scale by effects of the regional E-P budget. Conversely, the δ^{13}C signal in the Tethyan region seems to document more precisely the effects of a progressive isolation of this area from the deep global circulation system. The direct response of the productivity at Massignano to the progressive global climate cooling that occured prior to the Oi-1 event seems to suggest a permanent control of primary climate forcing on the biological dynamics and carbon cycle in the Tethyan region.

7. Conclusions

[51] The new magnetostratigraphic data set, combined with the results of the astronomical tuning on the Massignano section [*Jovane et al.*, 2006], allows us to refine the dates for the bio- and chrono-stratigraphic events recorded previously throughout the succession (Table 1 and Figure 10). A primary change is in the age of the Eocene-Oligocene boundary, which is placed at 33.7 Ma, 0.2 m.y. younger than in the recent timescale of *Gradstein et al.* [2004].

[52] The rock magnetic properties of the Massignano section are distinctly bimodal with abrupt transitions between modes. The mechanism driving these changes in properties apparently switches on and off fairly rapidly. We

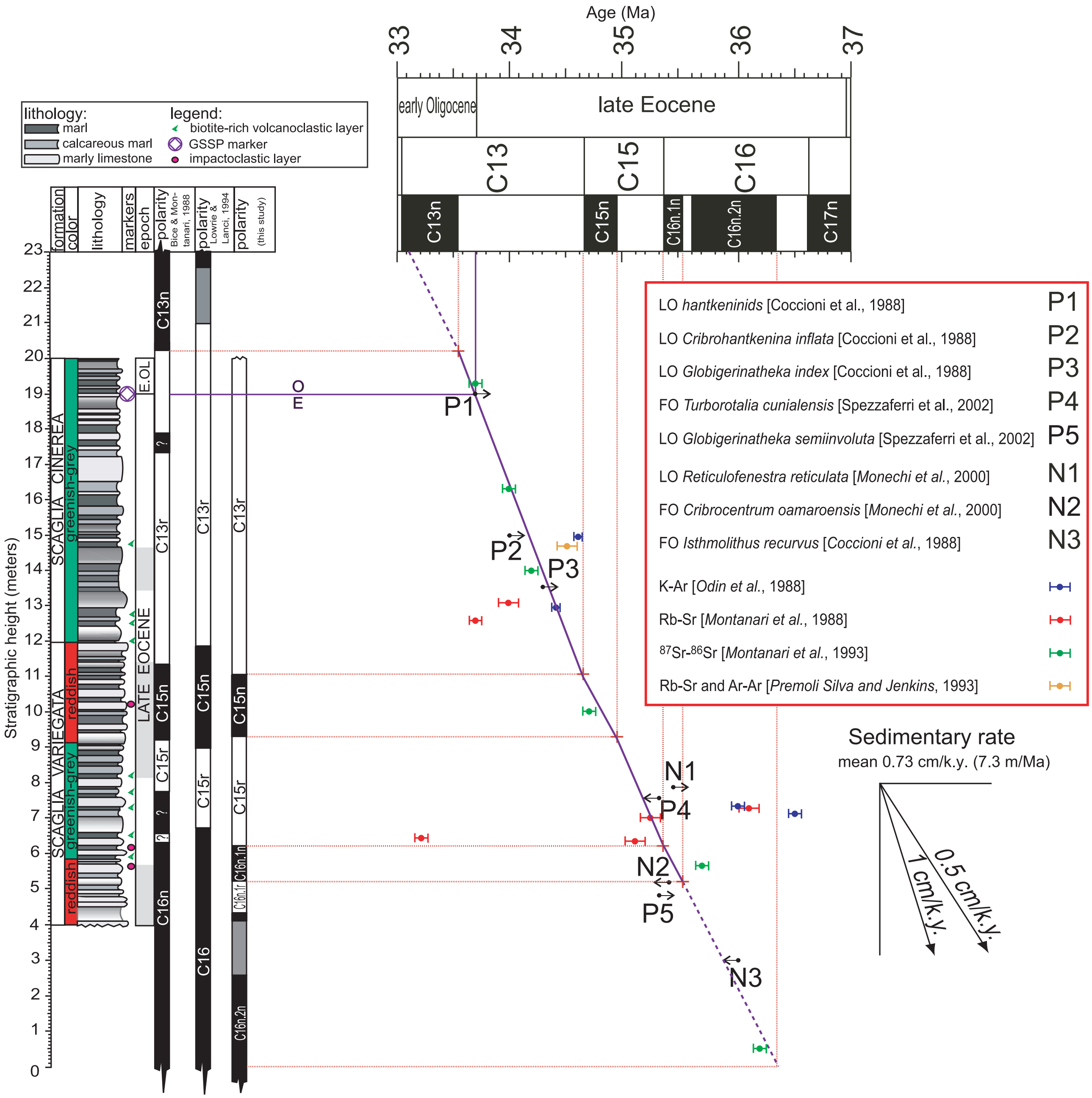

Figure 10. Age vs. stratigraphic height plot with correlation of the polarity zonation to the GPTS of *Cande and Kent* [1995]. Both geochronological [*Montanari et al.*, 1988, 1993; *Odin et al.*, 1988; *Premoli Silva and Jenkins*, 1993], and microfossil: calcareous nannofossil (N) [*Coccioni et al.*, 1988; *Monechi et al.*, 2000] and planktonic foraminiferal (P) [*Coccioni et al.*, 1988; *Spezzaferri et al.*, 2002] data are used to constrain the interpretation. The sedimentation rate along the section oscillates from 0.6 to 0.8 cm/k.y., with a mean, calculated by linear interpolation between consecutive reversal boundaries, of 0.73 cm/k.y. Previously, *Premoli Silva and Jenkins* [1993] obtained a single radiometric date of 34.6 (±0.3) Ma at 14.7 msl, which is 4.3 m below the E/O boundary. Using this datum and a constant sedimentation rate (0.71 cm/k.y.), they estimated the age of the E/O boundary at 34 (±0.1) Ma. Later, *Gradstein et al.* [2004] revised the age to 33.9 Ma. The astronomical tuning of the record [*Jovane et al.*, 2006] places the E/O boundary at 33.71 Ma in excellent agreement with an estimated age of 33.70 ± 0.03 m.y. defined only by linear interpolation through the base of Chron 13n [*Lowrie and Lanci*, 1994] and the top of Chron 15n (this work). The small uncertainty is based only on relative errors. The uncertainty in the absolute age is larger and depends on the uncertainty in the ages of the polarity boundaries of the GPTS, which are not well quantified but are >0.1 m.y.

suggests that the mechanism that drives the changes in concentration, composition, and grain-size of the magnetic minerals, while clay minerals abundances and calcium carbonate content remain constant, is related to paleoceanographic events that occurred in the deep-sea environment. Stable isotope analysis on ostracod shells reinforce this hypothesis showing similar variations that could be only related to bottom water evolution. Therefore we suggest that the late Eocene long-term magnetic mineral and stable isotope variations at Massignano might be primarily related to the long-term variations in bottom sea ventilation.

[53] The magnetic mineral properties in some periods are an expression of changes of deep-sea conditions and freshening in relation to the ocean paleo-currents through the Neo-Tethys during the Eocene [e.g., *Coccioni et al.*, 2000; *Dall'Antonia et al.*, 2002; *Harzhauser et al.*, 2002; *Coccioni and Galeotti*, 2003; *Verducci and Nocchi*, 2004]. The fact that the fine magnetic minerals decrease towards the top of the section suggests that those paleo-oceanic conditions were ending.

[54] **Acknowledgments.** We appreciate the insightful comments by Benjamin Cramer, the two anonymous reviewers and anonymous Associate Editor. This is contribution no. 17 of the Centro di Geobiologia of the Urbino University.

References

Acton, G., A. Roth, and K. L. Verosub (2007), Analyzing micromagnetic properties with FORCIT software, *Eos*, *88*, 230.

Barker, P. F., and E. Thomas (2004), Origin, signature and palaeoclimatic influence of the Antarctic Circumpolar Current, *Earth-Sci. Rev.*, *66*, 143–162.

Barker, P. F., G. M. Filippelli, F. Florindo, E. E. Martin, and H. D. Scher (2007), Onset and Role of the Antarctic Circumpolar Current, *Deep Sea Res. II*, in press.

Berggren, W. A., D. V. Kent, C. C. Swisher III, and M. P. Aubry (1995), A revised Cenozoic geochronology and chronostratigraphy, in *Geochronology, Time Scales and Global Stratigraphic Correlation: SEPM Special Publication*, vol. 54, edited by W. A. Berggren, D. V. Kent, M. P. Aubry, and J. Hardenbol, pp. 129–212.

Besse, J., and V. Courtillot (1991), Revised and synthetic apparent polar wander paths of the African, Eurasian, North American and Indian Plates, and true polar wander since 200 Ma, *J. Geophys. Res.*, *96*, 4029–4050.

Bice, D. M., and A. Montanari (1988), Magnetic stratigraphy of the Massignano section across the Eocene–Oligocene boundary, in *International Subcommission on Paleogene Stratigraphy*, edited by I. Premoli Silva, R. Coccioni, and A. Montanari, pp. 111–118, Industrie Grafiche Fratelli Aniballi, Ancona.

Bodiselitsch, B., A. Montanari, C. Koeberl, and R. Coccioni (2004), Delayed climate cooling in the Late Eocene caused by multiple impacts: High-resolution geochemical studies at Massignano, Italy, *Earth Planet. Sci. Lett.*, *223*(3–4), 283–302.

Bohaty, S. M., and J. C. Zachos (2003), Significant southern ocean warming event in the late middle Eocene, *Geology*, *31*, 1017–1020.

Brinkhuis, H., and H. Visscher (1995), The upper boundary of the Eocene Series; a reappraisal based on dinoflagellate cyst biostratigraphy and sequence stratigraphy, in *Geochronology, Time Scales and Global Stratigraphic Correlation: SEPM Special Publication*, vol. 54, edited by W. A. Berggren, D. V. Kent, M. P. Aubry, and J. Hardenbol, pp. 129–212.

Cande, S. C., and D. V. Kent (1995), Revised calibration of the geomagnetic polarity time scale for the Late Cretaceous and Cenozoic, *J. Geophys. Res.*, *100*, 6093–6095.

Coccioni, R., and S. Galeotti (2003), Deep-water benthic foraminiferal events from the Massignano Eocene/Oligocene Boundary Stratotype Section and Point (central Italy): biostratigraphic, paleoecologic, and paleoceanographic implications, in *From Greenhouse to Icehouse: The Marine Eocene-Oligocene Transition*, edited by D. R. Prothero, L. C. Ivant, E. Nesbitt, pp. 438-452, Columbia Univ. Press, New York.

Coccioni, R., P. Monaco, S. Monechi, M. Nocchi, and G. Parisi (1988), Biostratigraphy of the Eocene/Oligocene boundary at Massignano (Ancona, Italy), in *International Subcommission on Paleogene Stratigraphy*, edited by I. Premoli Silva, R. Coccioni, and A. Montanari, pp. 50-80, Industrie Grafiche F.lli Aniballi, Special Publication, Ancona.

Coccioni, R., D. Basso, H. Brinkhuis, S. Galeotti, S. Gardin, S. Monechi, and S. Spezzaferri (2000), Marine biotic signal across a late Eocene impact layer at Massignano, Italy: Evidence for long-term environmental perturbations?, *Terra Nova*, *12*, 258–263.

Coxall, H. K., P. A. Wilson, H. Pälike, C. H. Lear, and J. Backman (2005), Rapid stepwise onset of Antarctic glaciation and deeper calcite compensation in the Pacific Ocean, *Nature*, *433*, 53–57.

Dall'Antonia, B., A. Bossio, and C. Guernet (2002), The Eocene/Oligocene and the psycrospheric event in the Tethys as recorded by deep-sea ostracods from the Massignano Global Boundary Stratotype Section and Point, Central Italy, *Mar. Micropaleontol.*, *910*, 1–16.

DeConto, R. M., and D. Pollard (2003), Rapid Cenozoic glaciation of Antarctica induced by declining atmospheric CO_2, *Nature*, *421*, 245–249.

Dekkers, M. J., C. G. Langereis, S. P. Vriend, P. J. M. van Santvoort, and G. J. De Lange (1994), Fuzzy c-means cluster analysis of early diagenetic effects on natural remanent magnetisation acquisition in a 1.1 Myr piston core from the central Mediterranean, *Phys. Earth Planet. Inter.*, *85*, 155–171.

Dercourt, J., M. Gaetani, B. Vrielynck, E. Barrier, B. Biju-Duval, M. F. Brunet, J. P. Cadet, S. Crasquin and M. Sandulescu (2000), 24 maps, *Peri-Tethys Atlas Palaeogeographical maps*, CCGM, Paris, France.

Diester-Haass, L., and R. Zahn (1996), Eocene-Oligocene transition in the Southern Ocean: History water mass circulation and biological productivity, *Geology*, *24*, 163–166.

Gonzalez, R. C., and R. E. Woods (1992), *Digital image processing*, Addison Wessley Publishing Company, ISBN 0202508036, New York.

Gradstein, F. M., J. G. Ogg, and A. G. Smith (2004), *A Geological Time Scale 2004*, 589 pp., Cambridge Univ. Press, Cambridge.

Hanesch, M., R. Scholger, and M. J. Dekkers (2001), The application of fuzzy C-Means cluster analysis and non-linear mapping to a soil data set for the detection of polluted sites, *Phys. Chem. Earth*, *26*, 885–891.

Harzhauser, M., W. E. Piller, and F. F. Steininger (2002), Circum-Mediterranean Oligo-Miocene biogeographic evolution - The gastropods' point of view, *Palaeogeogr. Palaeoclimatol. Palaeoecol.*, *183*, 103–133.

Hopkinson, J. (1889), Magnetic and other physical properties of iron at high temperature, *Phil. Trans. R. Soc.*, *A180*, 443–465.

Hrouda, F. (1994), A technique for the measurement of thermal changes of magnetic susceptibility of weakly magnetic rocks by the CS-2 apparatus and KLY-2 Kappabridge, *Geophys. J. Int.*, *118*, 604–612.

Hu, X., L. Jansa, and M. Sarti (2005), Mid-Cretaceous oceanic red beds in the Umbria–Marche Basin, central Italy: Constraints on paleoceanography and paleoclimate, *Palaeogeogr. Palaeoclimatol. Palaeoecol.*, *233*, 163–186.

Jovane, L., F. Florindo, and J. Dinarès-Turell (2004), Environmental magnetic record of paleoclimate change from the Eocene-Oligocene stratotype section, Massignano, Italy, *Geophys. Res. Lett.*, *31*, L15601, doi:10.1029/2004GL020554.

Jovane, L., F. Florindo, M. Sprovieri, and H. Pälike (2006), Astronomic calibration of the late Eocene/early Oligocene Massignano section (central Italy), *Geochem. Geophys. Geosyst.*, *7*(7), Q07012, doi:10.1029/2005GC001195.

Jovane, L., F. Florindo, J. Dinarès-Turell, A. Marsili, R. Coccioni, S. Monechi, A. P. Roberts, and M. Sprovieri (2007), Evidences of the middle Eocene Climatic Optimum (MECO) event from the Contessa Highway section, Umbrian Apennines, Italy, *Geol. Soc. Am. Bull.*, *119*(3/4), 413–427, doi:10.1130/B25917.1.

Kennett, J. P., and N. J. Shackleton (1976), Oxygen isotopic evidence for development of the psychrosphere 38 Myr ago, *Nature*, *260*, 513–515, doi:10.1038/260513a0.

Kirschvink, J. L. (1980), The least-squares line and plane and the analysis of paleomagnetic data, *Geophys. J.R. Astron. Soc.*, *62*, 699–718.

Lanci, L., and W. Lowrie (1997), Magnetostratigraphic evidence that 'tiny wiggles' in the oceanic magnetic anomaly record represent geomagnetic paleointensity variations, *Earth and Planet. Sci. Lett.*, *148*, 581–592.

Lanci, L., W. Lowrie, and A. Montanari (1996), Magnetostratigraphy of the Eocene/Oligocene boundary in a short drill-core, *Earth Planet. Sci. Lett.*, *143*, 37–48.

Lanci, L., W. Lowrie, and A. Montanari (1998), Stratigrafia magnetica ad alta risoluzione del limite Eocene-Oligocene nella successione Umbro-Marchigiana, *Atti della Accademia Nazionale dei Lincei*, *Rend. Fis. Acc. Lincei*, *9*, 109–129.

Lawver, L. A., and L. M. Gahagan (2003), Evolution of Cenozoic seaways in the circum-Antarctic region, *Palaeogeogr. Palaeoclimatol. Palaeoecol.*, *198*, 11–37.

Lear, C. H., H. Elderfield, and P. A. Wilson (2000), Cenozoic deep-sea temperatures and global ice volumes from Mg/Ca in benthic foraminiferal calcite, *Science*, *287*, 269–272.

Livermore, R., A. Nankivell, G. Eagles, and P. Morris (2005), Paleogene opening of Drake Passage, *Earth Planet. Sci. Lett.*, *236*, 459–470.

Livermore, R., C.-D. Hillenbrand, M. Meredith, and G. Eagles (2007), Drake Passage and Cenozoic climate: An open and shut case?, *Geochem. Geophys. Geosyst.*, *8*, Q01005, doi:10.1029/2005GC001224.
Lowrie, W. (1990), Identification of ferromagnetic minerals in a rock by coercivity and unblocking temperature properties, *Geophys. Res. Lett.*, *17*, 159–162.
Lowrie, W., and L. Lanci (1994), Magnetostratigraphy of Eocene-Oligocene boundary sections in Italy: No evidence for short subchrons within chrons 12R and 13R, *Earth Planet. Sci. Lett.*, *126*, 247–258.
Mattias, P., G. Crocetti, E. Barrese, A. Montanari, R. Coccioni, P. Farabollini, and E. Parisi (1992), Caratteristiche mineralogiche e lithostratigrafiche della sezione eo-oligocenica di Massignano (Ancona, Italia) comprendente il limite Scaglia Variegata-Scaglia Cinerea, *Studi Geol. Camerti*, *12*, 93–103.
Miller, K. G., J. D. Wright, and R. G. Fairbancks (1991), Unlocking the ice house: Oligocene-Miocene oxygen isotopes, eustacy and margin erosion, *J. Geophys. Res.*, *96*, 6829–6848.
Miller, K. G., J. D. Wright, and J. V. Browning (2005a), Visions of ice sheets in a greenhouse world, Marine, *Geology*, *217*, 215–231.
Miller, K. G., M. A. Kominz, J. V. Browning, J. D. Wright, G. S. Mountain, M. E. Katz, P. J. Sugarman, B. S. Cramer, N. Christie-Blick, and S. F. Pekar (2005b), The Phanerozoic record of global sea-level change, *Science*, *310*, 1293–1298.
Monechi, S., A. Buccianti, and S. Gardin (2000), Biotic signals from nannoflora across the iridium anomaly in the upper Eocene of the Massignano section: Evidence from statistical analysis, *Mar. Micropaleontol.*, *39*, 219–237.
Montanari, A., and C. Koeberl (2000), Impact stratigraphy: The Italian record, *Lecture Notes in Earth Sciences*, *93*, 364 pp., Springer, Heidelberg.
Montanari, A., A. L. Deino, R. E. Drake, B. D. Turrin, D. J. De Paolo, G. S. Odin, G. H. Curtis, W. Alvarez, and D. M. Bice (1988), Radioisotopic dating of the Eocene-Oligocene boundary in the pelagic sequence of the northeastern apennineds, in *The Eocene/Oligocene Boundary in the Marche-Umbria Basin (Italy): International Subcommission on Paleogene Stratigraphy, special publication*, edited by I. Premoli Silva, R. Coccioni, and A. Montanari, pp. 195–208, Industrie Grafiche Fratelli Aniballi, Ancona, Italy.
Montanari, A., F. Asaro, H. V. Michel, and J. P. Kennett (1993), Iridium anomalies of late Eocene age at Massignano (Italy), and ODP 689B (Maud Rise, Antarctic), *Palaios*, *8*, 420–437.
Odin, G. S., S. Clauser, and M. Renard (1988), Sedimentological and geochemical data on the Eocene – Oligocene boundary at Massignano (Apennines, Italy), in *International Subcommission on Paleogene Stratigraphy*, edited by I. Premoli Silva, R. Coccioni, and A. Montanari, pp. 175–186, Industrie Grafiche F.lli Aniballi, Special Publication, Ancona.
Opdyke, N. D., and J. E. T. Channell (1996), *Magnetic Stratigraphy*, 64 pp., edited by R. Dmowska and J. R. Holton, International Geophysics Series, Academic Press, Burlington (MA).
Pagani, M., J. C. Zachos, K. H. Freeman, B. Tipple, and S. Bohaty (2005), Marked decline in atmospheric carbon dioxide concentrations during the Paleogene, *Science*, *309*, 600–603.
Pearson, P. N., P. W. Ditchfield, J. Singano, K. G. Harcourt-Brown, C. J. Nicholas, R. K. Olsson, N. J. Shackleton, and M. A. Hall (2001), Warm tropical sea surface temperatures in the Late Cretaceous and Eocene epochs, *Nature*, *413*, 481–487.
Premoli Silva, I., and D. G. Jenkins (1993), Decision on the Eocene-Oligocene boundary stratotype, *Episodes*, *16*, 379–382.
Premoli Silva, I., R. Coccioni, and A.Montanari (1988), *The Eocene/Oligocene Boundary in the Marche-Umbria Basin (Italy): International Subcommission on Paleogene Stratigraphy, special publication*, pp. 195–208, Industrie Grafiche Fratelli Aniballi, Ancona, Italy.
Spezzaferri, S., D. Basso, and R. Coccioni (2002), Late Eocene planktonic foraminiferal response to an extraterrestrial impact at Massignano GSSP (northeastern Apennines, Italy), *J. Foraminiferal Res.*, *32*, 188–199.
Spötl, C., and T. W. Vennemann (2003), Continuous-flow isotope ratio mass spectrometric analysis of carbonate minerals, *Rapid Comm. Mass Spectrom.*, *17*, 1004–1006.
Stoner, J. S., J. E. T. Channell, and C. Hillaire-Marcel (1996), The magnetic signature of rapidly deposited detrital layers from the deep Labrador Sea: Relationship to North Atlantic Heinrich layers, *Paleoceanography*, *11*, 309–325.
Tripati, A. K., M. L. Delaney, J. C. Zachos, L. D. Anderson, D. C. Kelly, and H. Elderfield (2003), Tropical sea-surface temperature reconstruction for the early Paleogene using Mg/Ca ratios of planktonic foraminifera, *Paleoceanography*, *18*(4), 1101, doi:10.1029/2003PA000937.
Tripati, A. K., J. Backman, H. Elderfield, and P. Ferretti (2005), Eocene bipolar glaciation associated with global carbon cycle changes, *Nature*, *436*, 341–346.
Venuti, V., F. Florindo, E. Michel, and I. R. Hall (2007), Magnetic proxy for the deep (Pacific) western boundary current variability across the mid-Pleistocene climate transition, *Earth Planet. Sci. Lett*, doi:10.1016/j.epsl.2007.04.032.
Verducci, M., and M. Nocchi (2004), Middle to Late Eocene main planktonic foraminiferal events in the Central Mediterranean area (Umbria-Marche basin) related to paleoclimatic changes, *Neues Jahrbuch für Geologie und Paläontologie*, *Abhandlungen*, *234*, 361–413.
Vonhof, H. B., J. Smit, H. Brinkhuis, A. Montanari, and A. J. Nederbragt (2000), Global cooling accelerated by early late Eocene impacts?, *Geology*, *28*, 687–690.
Wade, B. S., and H. Pälike (2004), Oligocene climate dynamics, *Paleoceanography*, *19*, PA4019, doi:10.1029/2004PA001042.
Zachos, J. C., L. D. Stott, and K. C. Lohmann (1994), Evolution of early Cenozoic marine temperatures, *Paleoceanography*, *9*, 353–387.
Zachos, J. C., T. M. Quinn, and K. A. Salamy (1996), High Resolution (104 years) deep sea foraminiferal stable isotope records of the Eocene-Oligocene climate transitions, *Paleoceanography*, *11*, 251–266.
Zachos, J. C., M. Pagani, L. Sloan, E. Thomas, and K. Billups (2001), Trends, rhythms, and aberrations in global climate 65 Ma to Present, *Science*, *292*, 686–693.
Zijderveld, J. D. A. (1967), A.C. demagnetization of rocks, in *Analysis of results, in Methods in Paleomagnetism*, edited by D. W. Collinson, pp. 254–286, Elsevier Sciences, New York.

G. Acton, Department of Geology, University of California, Davis, One Shields Avenue, 95616, Davis, CA, USA.

R. Coccioni, Istituto di Geologia e Centro di Geobiologia, Università degli Studi di Urbino "Carlo Bo", Campus Scientifico Località Crocicchia, 61029 Urbino, Italy.

B. Dall'Antonia, Università di Pisa, Dipartimento di Scienze della Terra, Via Santa Maria 53, 56126 Pisa, Italy.

J. Dinarès-Turell, F. Florindo, and L. Jovane, Istituto Nazionale di Geofisica e Vulcanologia, Via di Vigna Murata 605, 00143 Rome, Italy. (jovane@ingv.it)

M. Sprovieri, Istituto Ambiente Marino Costiero (CNR), Calata Porta di Massa (Interno Porto di Napoli), 80133 Naples, Italy.